

Meiotic chromosome structures constrain and respond to designation of crossover sites

Diana E. Libuda¹, Satoru Uzawa², Barbara J. Meyer² & Anne M. Villeneuve^{1,3}

Crossover recombination events between homologous chromosomes are required to form chiasmata, temporary connections between homologues that ensure their proper segregation at meiosis I¹. Despite this requirement for crossovers and an excess of the double-strand DNA breaks that are the initiating events for meiotic recombination, most organisms make very few crossovers per chromosome pair². Moreover, crossovers tend to inhibit the formation of other crossovers nearby on the same chromosome pair, a poorly understood phenomenon known as crossover interference^{3,4}. Here we show that the synaptonemal complex, a meiosis-specific structure that assembles between aligned homologous chromosomes, both constrains and is altered by crossover recombination events. Using a cytological marker of crossover sites in *Caenorhabditis elegans*⁵, we show that partial depletion of the synaptonemal complex central region proteins attenuates crossover interference, increasing crossovers and reducing the effective distance over which interference operates, indicating that synaptonemal complex proteins limit crossovers. Moreover, we show that crossovers are associated with a local 0.4–0.5-micrometre increase in chromosome axis length. We propose that meiotic crossover regulation operates as a self-limiting system in which meiotic chromosome structures establish an environment that promotes crossover formation, which in turn alters chromosome structure to inhibit other crossovers at additional sites.

Although crossovers mature in the context of assembled synaptonemal complexes (SCs), whether the SC functions in crossover interference has long been debated^{6–8}. Largely on the basis of analysis in budding yeast, it has been argued for the last decade that the SC is irrelevant for interference⁶. Consequently, suggestive evidence that the SC might be involved in interference in other organisms has gained little traction^{9,10}. The debate persists in part because of inherent limitations of some assays used to score crossovers (see Supplementary Discussion). We overcome this problem by taking advantage of the fact that the *C. elegans* crossover-promoting protein COSA-1, which forms foci at nascent crossover sites *in vivo*, serves as a robust cytological marker of the crossovers that elicit and respond to crossover interference⁵.

C. elegans exhibits robust crossover interference, with chromosome pairs normally undergoing only a single crossover². Using COSA-1 foci, we assessed whether the SC central region proteins (the SYP proteins) function in limiting the number of crossovers per chromosome pair. SYPs are essential for crossover formation^{11–13}, precluding the use of *syp* null mutants for this analysis. To circumvent this issue, we used RNA interference (RNAi) to partially deplete SYP-1 protein levels by ~60–70% (Extended Data Fig. 1). In contrast to a previous study⁹, the residual SYP-1 levels achieved using our experimental conditions were sufficient to permit assembly of SCs (albeit with reduced ratios of SYPs to axis subunits) and formation of chiasmata for all six chromosome pairs in most gonads (see Supplementary Discussion and Methods). Although SYPs are required to form crossovers, we found that partial depletion of SYP-1, SYP-2 or SYP-3 increases COSA-1 foci (Fig. 1a and Extended Data Fig. 2), indicating

that a sufficient pool of SYPs is required to limit COSA-1-marked crossovers to one per chromosome pair.

In principle, an increase in COSA-1-marked crossover sites could reflect an increase in the number of double-strand breaks (DSBs) formed and/or an increase in the fraction of DSBs repaired as crossovers. Therefore, we controlled DSB number by using γ -irradiation to induce DSBs in *spo-11* mutant worms, which are proficient for pairing and SC assembly but lack endogenous meiotic DSBs (Fig. 1b)¹⁴. Controls recapitulated the previous finding that increasing DSBs beyond the level needed to ensure at least one per chromosome pair (1,000 Rad, 23.5 DSBs per nucleus) did not increase the average number of COSA-1 foci per nucleus beyond six⁵. Further, COSA-1 foci exhibited very low standard deviations (± 0.14 – 0.27), reflecting operation of the robust crossover control system. By contrast, upon *syp-1* RNAi, most nuclei

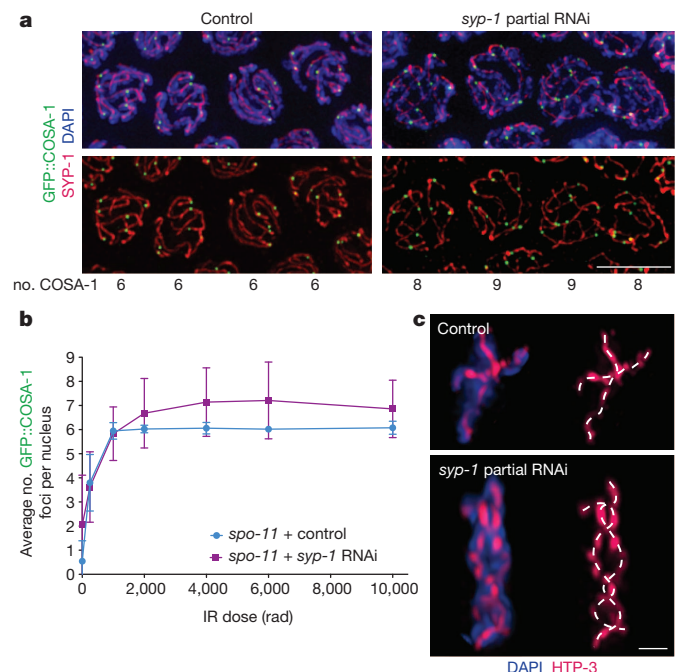


Figure 1 | SYP-1 partial depletion increases numbers of COSA-1 foci and chiasmata. **a**, Immunofluorescence images of late pachytene nuclei from control or *syp-1* partial RNAi worms. DAPI, 4',6-diamidino-2-phenylindole. Scale bar, 5 μ m. **b**, Dose–response graph depicting mean numbers of green fluorescent protein (GFP)::COSA-1 foci formed per nucleus in response to DSBs generated by increasing doses of γ -irradiation (IR, rad). See Methods for numbers of nuclei used; error bars indicate \pm s.d. At >1,000 rad, both the mean numbers of foci and s.d. were increased in *syp-1* RNAi relative to control. **c**, Three-dimensionally rendered images of individual diakinesis bivalents comprising the *mnt12* (*X;IV*) fusion chromosome pair. Dashed lines (white) indicate traced HTP-3 axes, with crossing of axes indicating chiasmata. Scale bar, 1 μ m.

¹Department of Developmental Biology, Stanford University, School of Medicine, Stanford, California 94305, USA. ²Howard Hughes Medical Institute and Department of Molecular and Cell Biology, University of California at Berkeley, Berkeley, California 94720, USA. ³Department of Genetics, Stanford University, School of Medicine, Stanford, California 94305, USA.

exposed to $>1,000$ rad of γ -irradiation had >6 COSA-1 foci and standard deviations were much higher (± 1.2 – 1.6), indicating impairment of crossover control. This experiment shows that increased DSBs alone cannot account for the increase in COSA-1 foci following SYP-1 partial depletion, and that for any given level of DSBs, SYP-1 has a role in determining the fraction that will mature into cytologically differentiated crossovers.

Our data suggest that SYP-1 partial depletion impairs crossover interference. To investigate this further, we used worms homozygous for the two-chromosome fusion *mnT12* (X chromosome fused with chromosome IV)^{10,15}. Previous work showed that although crossover interference limits the *mnT12* chromosome pair to a single COSA-1 focus in the majority of meioses, *mnT12* chromosome pairs with two COSA-1 foci also occur⁵. Under our control conditions, 51% of *mnT12* pairs had a single COSA-1 focus, whereas 49% had two foci (Fig. 2a, b and Methods). This occurrence of two COSA-1 foci along *mnT12* allowed us to assess interference strength in the context of wild-type SYP-1 levels and compare it to crossover/chiasma interference in the context of SYP-1 partial depletion (Figs 1c and 2–4).

Increased COSA-1 foci following *syp-1* RNAi correlated with an increased number of cytologically resolvable chiasmata on *mnT12* bivalents at diakinesis, the last stage of prophase (Fig. 1c and Extended Data Fig. 3). Consistent with *mnT12* having only one or two COSA-1 foci at the late pachytene stage in controls (average of 1.49 COSA-1 foci per *mnT12* pair), control *mnT12* diakinesis bivalents had only one or two chiasmata. Upon *syp-1* RNAi, an average of 2.57 COSA-1 foci per *mnT12* pair were observed at late pachytene (49% having ≥ 3 foci; Fig. 2b), and 47% of diakinesis bivalents had ≥ 3 chiasmata. These and other data (Extended Data Fig. 3) indicate that the extra COSA-1 foci in *syp-1* RNAi worms represent bona fide cytologically differentiated inter-homologue crossovers.

We conducted quantitative analyses evaluating the positions, distributions and distances between COSA-1-marked sites on computationally straightened *mnT12* chromosomes (with HTP-3 immunofluorescence marking chromosome axes¹⁶ and with immunofluorescence for the HIM-8 protein, which localizes near the left end of the X chromosome¹⁷, serving as an orientation marker; Fig. 2a and Methods). The average distance between COSA-1 foci on *mnT12* with ≥ 2 COSA-1 foci in *syp-1* RNAi was $4.5 \mu\text{m}$, substantially shorter than the average distance of $8.5 \mu\text{m}$ for control *mnT12* with two foci ($P < 0.0001$). Further, even when only *syp-1* RNAi *mnT12* with two foci were considered, the average distance ($6.5 \mu\text{m}$) was still significantly shorter than in controls ($P < 0.0001$; Fig. 2c). These data show that *syp-1* RNAi decreases the effective distance over which interference operates. The average distance between COSA-1 foci on control *mnT12* ($8.5 \mu\text{m}$) exceeds the average axis length of unfused autosomes ($6.4 \mu\text{m}$, $P < 0.0001$), reinforcing the indirect inference from ref. 10 that interference in *C. elegans* operates over distances longer than the length of a normal chromosome.

We assessed crossover interference further by dividing the *mnT12* axis into eight evenly spaced intervals and binning the positions of COSA-1 foci into these intervals (Fig. 2d, e and Extended Data Fig. 4). First, we compared the distributions of COSA-1 foci among these intervals for chromosomes with different numbers of foci. In controls, COSA-1 foci exhibited a specific non-random distribution indicative of interference: for the subset of chromosomes with only one COSA-1 focus, the single focus usually occurred near the middle of *mnT12*, whereas for the subset of chromosomes with two COSA-1 foci, those foci predominantly occurred near the chromosome ends (Fig. 2d). By contrast, *syp-1* RNAi resulted in a fairly even distribution of foci along *mnT12*, regardless of the number of COSA-1 foci, consistent with attenuation of crossover interference. Second, plotting the separation between adjacent pairs of COSA-1 foci (Fig. 2e) revealed wide spacing (≥ 4 interval boundaries) separating adjacent COSA-1 foci in controls, and reduced separation between adjacent foci in *syp-1* RNAi worms, both when all pairs of foci or only chromosomes with two foci were considered.

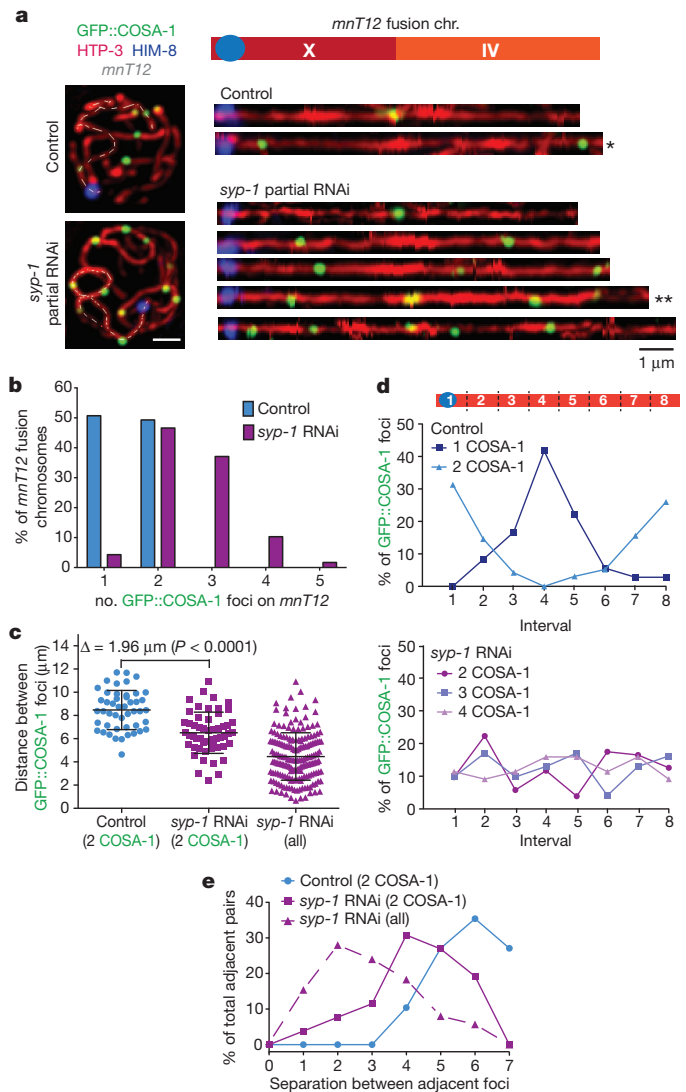


Figure 2 | SYP-1 partial depletion attenuates crossover interference. **a**, Left, projections of individual late pachytene nuclei containing the *mnT12* fusion chromosome (depicted schematically at top right), which is identified by its associated HIM-8 focus; grey dotted line indicates the traced three-dimensional path of the *mnT12* chromosome axis. Right, representative computationally straightened *mnT12* used for quantitative analyses in **b–e** and Figs 3 and 4. Asterisks indicate the straightened chromosomes from the nuclei shown. Scale bars, $1 \mu\text{m}$. **b**, Graph indicating the percentage of *mnT12* with the indicated number of COSA-1 foci for control ($n = 69$) and *syp-1* RNAi ($n = 115$). **c**, Scatterplot showing measured distances (μm) between COSA-1 foci on control *mnT12* with two foci, on *syp-1* RNAi *mnT12* with two foci, and on all *syp-1* RNAi *mnT12* with multiple foci. Horizontal lines indicate the mean; error bars indicate s.d. **d**, Graphs indicating the distributions of foci among eight evenly spaced intervals along the *mnT12* axis (schematic at top) for the subsets of control (top graph) and *syp-1* RNAi (bottom graph) *mnT12* with the indicated numbers of COSA-1 foci. **e**, Graph depicting the distributions of spacing between adjacent pairs of foci. Using the same eight-interval scheme as in **d**, separation values are defined as the number of interval boundaries crossed before encountering the next focus (that is, adjacent foci within the same interval on the same chromosome pair have a separation of 0, adjacent foci in consecutive intervals have a separation of 1, etc.). See Methods for numbers of *mnT12* chromosomes used for **c–e**.

We also used two quantitative methods to calculate interference strength. First, we performed a coefficient of coincidence analysis, with *mnT12* divided into four intervals (Fig. 3a, Extended Data Fig. 4, Extended Data Table 1 and Methods). Controls exhibit a robust signature of interference (I): complete interference ($I = 1$) for adjacent interval pairs; strong but reduced interference for pairs at intermediate

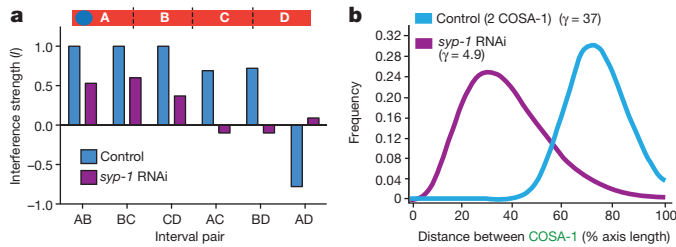


Figure 3 | SYP-1 partial depletion decreases crossover interference strength. **a**, Graph of interference strength (I) values for the indicated interval pairs, where $I = 1 - \text{observed/expected}$ (Methods); schematic (top) indicates division of *mnT12* into four intervals for this analysis. **b**, Graph showing best-fit probability density function curves generated when a gamma distribution was used to model the distribution of inter-focus distances; for this analysis, distances between adjacent foci were expressed as percentage of axis length. See Methods for numbers of chromosomes used.

distance; and high ‘negative’ interference ($I < 0$) for the pair of intervals including opposite ends of the chromosome, indicating that a chromosome with a focus in one end-interval has an increased likelihood of a second focus in the opposite end-interval (Fig. 2d, top). By contrast, the *syp-1* RNAi data show reduced interference for adjacent interval pairs, and no interference for interval pairs separated by ≥ 1 interval, indicating attenuated interference. Second, we used a gamma distribution to model inter-focus distances (expressed as a percentage of total axis length), and generated best-fit probability density curves where the shape parameter (γ) is a relative indicator of interference strength, with $\gamma = 1$ indicating no interference and higher values signifying stronger interference¹⁸ (Fig. 3b and Extended Data Fig. 5). Whereas the control displayed very strong interference ($\gamma = 37$), *syp-1* RNAi displayed a substantial attenuation of interference ($\gamma = 4.9$).

A separate analysis of our *mnT12* data yielded another key finding: COSA-1-marked crossovers are associated with a local increase in chromosome axis length (Fig. 4). Plotting the mean axis length for *syp-1* RNAi *mnT12* with 1, 2, 3 or 4 foci revealed a striking linear relationship between number of COSA-1 foci and mean axis length ($R^2 = 0.952$), with the slope of the linear regression line indicating that each COSA-1 focus is associated with a 0.4- μm increase in axis length (Fig. 4a). Further, association between number of foci and axis length was also observed in controls (Fig. 4a). Moreover, comparison of *mnT12* axis lengths in a *spo-11* mutant (which lacks crossovers) and in *spo-11/+* heterozygous controls yielded a similar linear relationship for *mnT12* with 0, 1 or 2 COSA-1 foci (Fig. 4b; slope = 0.49, $R^2 = 0.952$). Analysis of unfused autosomes from *spo-11*, controls and *syp-1* RNAi worms likewise showed each COSA-1 focus associating with a 0.4- μm increase in axis length (Fig. 4c; $R^2 = 0.999$), demonstrating that the relationship between crossovers and axis length is generalizable to other chromosomes. Together, these data indicate that extension of chromosome axes occurs in response to crossover designation. Finally, assessment of the distance between the left end of the chromosome and the position of the HIM-8 focus on control *mnT12* (Fig. 4d and Extended Data Fig. 6) revealed that the mean length of this specific short axis segment was increased by 0.4–0.5 μm when a COSA-1 focus was present in the segment. As this value is comparable to that inferred from the linear regression analyses, we conclude that the increase in axis length associated with each crossover is predominantly a local effect.

Our demonstration that partial depletion of SYPs attenuates the robust crossover interference in *C. elegans* indicates a role for SC central region proteins in crossover control. This effect of SYP depletion on interference could reflect a decreased ability to propagate an inhibitory signal, a reduced sensitivity of recombination precursors to inhibition, and/or a prolonged state of competence for crossover designation. Our finding that SC central region subunits have a role in achieving the high level of interference characteristic of *C. elegans* meiosis can be reconciled with studies concluding that the SC is dispensable for

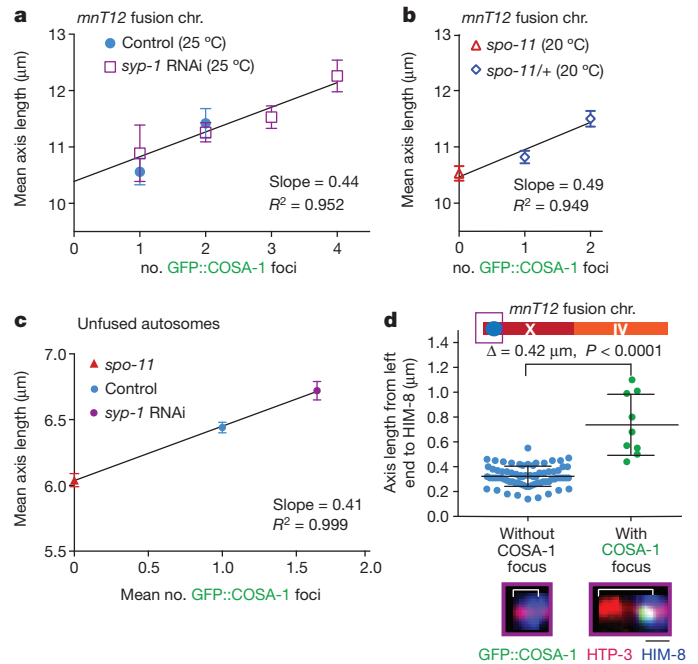


Figure 4 | Crossover designation causes a local expansion of chromosome axis length. **a**, **b**, Graphs plotting the relationship between number of COSA-1 foci and mean length (\pm s.e.m.) of the *mnT12* chromosome axis. **a**, Data for *syp-1* RNAi and control at 25 °C; extrapolated linear regression line was generated using the *syp-1* RNAi data. **b**, Data for *spo-11* and *spo-11/+* control at 20 °C. **c**, Graph plotting the relationship between mean number of COSA-1 foci and mean axis length (\pm s.e.m.) for unfused autosomes in *spo-11*, control and *syp-1* RNAi nuclei (Methods). **d**, Scatterplot showing length measurements (from control nuclei at 25 °C) for the axis segment extending from left end of *mnT12* to the centre of the HIM-8 focus for chromosomes that either lacked or had a COSA-1 focus in this segment, as depicted in images below the graph. Horizontal lines indicate mean; error bars indicate s.d. See Methods for numbers of chromosomes used.

interference in budding yeast^{19–21}, on the basis of several considerations. There is a growing body of evidence that, at least in some organisms, non-random distribution of prospective crossover intermediates may occur in (at least) two different steps^{22–24}. This suggests that multiple layers of regulation can contribute to the final interference distribution of crossovers, raising the possibility that the relative contributions of different crossover control mechanisms may differ between organisms. Thus, given that the attenuated interference observed following SYP-1 partial depletion in *C. elegans* ($\gamma = 4.9$) appears at least as strong or stronger than the interference observed in wild-type budding yeast ($\gamma = 1.9$)²⁵, we suggest that *C. elegans* may use a layer of crossover control that does not make an appreciable contribution in budding yeast.

Integrating our findings with previous data showing that crossover designation in *C. elegans* occurs in the context of assembled SCs^{5,26}, we suggest a model in which crossover designation requires a capacity for local expansion of previously assembled meiotic chromosome structures. We suggest that local expansion in turn alters the thickness, density and/or rigidity of structures beyond the local area, thereby reducing the capacity for axis expansion at other sites (see Supplementary Discussion). Overall, our work supports the idea that meiotic crossover regulation operates as a self-limiting system in which meiotic chromosome structures create an environment that promotes crossovers, which in turn modify chromosome structures to inhibit crossover formation at additional neighbouring sites.

METHODS SUMMARY

For assessing the effects of partial depletion of SYP-1, worms were exposed to RNAi treatment at 25 °C from the L1 stage until 16–22 h post-L4 stage, when their gonads were then dissected and processed for immunofluorescence. For Fig. 1,

chromosomes in three-dimensionally preserved meiotic prophase nuclei were imaged using wide-field deconvolution microscopy. For analyses involving measurements of chromosome axis lengths and positions of GFP::COSA-1 foci (Figs 2–4), three-dimensionally preserved nuclei were imaged using confocal microscopy, followed by three-dimensional tracing and subsequent computational straightening of chromosomes before recording of position coordinates²⁷. All *P* values reported in the main text are two-tailed and calculated from Mann–Whitney tests.

Online Content Any additional Methods, Extended Data display items and Source Data are available in the online version of the paper; references unique to these sections appear only in the online paper.

Received 25 April; accepted 16 August 2013.

Published online 9 October 2013.

- Page, S. L. & Hawley, R. S. Chromosome choreography: the meiotic ballet. *Science* **301**, 785–789 (2003).
- Martinez-Perez, E. & Colaiacovo, M. P. Distribution of meiotic recombination events: talking to your neighbors. *Curr. Opin. Genet. Dev.* **19**, 105–112 (2009).
- Muller, H. J. The mechanism of crossing-over. *Am. Nat.* **50**, 193–221 (1916).
- Sturtevant, A. H. The linear arrangements of six sex-linked factors in *Drosophila*, as shown by their mode of association. *J. Exp. Zool.* **14**, 43–59 (1913).
- Yokoo, R. *et al.* COSA-1 reveals robust homeostasis and separable licensing and reinforcement steps governing meiotic crossovers. *Cell* **149**, 75–87 (2012).
- Bishop, D. K. & Zickler, D. Early decision: meiotic crossover interference prior to stable strand exchange and synapsis. *Cell* **117**, 9–15 (2004).
- Egel, R. Synaptonemal complex and crossing-over: structural support or interference? *Heredity* **41**, 233–237 (1978).
- Maguire, M. P. Can abortive early homologous associations promote increased crossing-over in an adjacent rearranged segment? *Genome* **30**, 469–472 (1988).
- Hayashi, M., Mlynarczyk-Evans, S. & Villeneuve, A. M. The synaptonemal complex shapes the crossover landscape through cooperative assembly, crossover promotion and crossover inhibition during *Caenorhabditis elegans* meiosis. *Genetics* **186**, 45–58 (2010).
- Hillers, K. J. & Villeneuve, A. M. Chromosome-wide control of meiotic crossing over in *C. elegans*. *Curr. Biol.* **13**, 1641–1647 (2003).
- Colaiacovo, M. P. *et al.* Synaptonemal complex assembly in *C. elegans* is dispensable for loading strand-exchange proteins but critical for proper completion of recombination. *Dev. Cell* **5**, 463–474 (2003).
- MacQueen, A. J., Colaiacovo, M. P., McDonald, K. & Villeneuve, A. M. Synapsis-dependent and -independent mechanisms stabilize homolog pairing during meiotic prophase in *C. elegans*. *Genes Dev.* **16**, 2428–2442 (2002).
- Smolnikov, S. *et al.* SYP-3 restricts synaptonemal complex assembly to bridge paired chromosome axes during meiosis in *Caenorhabditis elegans*. *Genetics* **176**, 2015–2025 (2007).
- Dernburg, A. F. *et al.* Meiotic recombination in *C. elegans* initiates by a conserved mechanism and is dispensable for homologous chromosome synapsis. *Cell* **94**, 387–398 (1998).
- Sigurdson, D. C., Herman, R. K., Horton, C. A., Kari, C. K. & Pratt, S. E. An X-autosome fusion chromosome of *Caenorhabditis elegans*. *Mol. Gen. Genet.* **202**, 212–218 (1986).
- Goodyer, W. *et al.* HTP-3 links DSB formation with homolog pairing and crossing over during *C. elegans* meiosis. *Dev. Cell* **14**, 263–274 (2008).
- Phillips, C. M. *et al.* HIM-8 binds to the X chromosome pairing center and mediates chromosome-specific meiotic synapsis. *Cell* **123**, 1051–1063 (2005).
- McPeck, M. S. & Speed, T. P. Modeling interference in genetic recombination. *Genetics* **139**, 1031–1044 (1995).
- Fung, J. C., Rockmill, B., Odell, M. & Roeder, G. S. Imposition of crossover interference through the nonrandom distribution of synapsis initiation complexes. *Cell* **116**, 795–802 (2004).
- Börner, G. V., Kleckner, N. & Hunter, N. Crossover/noncrossover differentiation, synaptonemal complex formation, and regulatory surveillance at the leptotene/zygotene transition of meiosis. *Cell* **117**, 29–45 (2004).
- Storlazzi, A., Xu, L., Schwacha, A. & Kleckner, N. Synaptonemal complex (SC) component Zip1 plays a role in meiotic recombination independent of SC polymerization along the chromosomes. *Proc. Natl Acad. Sci. USA* **93**, 9043–9048 (1996).
- Cole, F. *et al.* Homeostatic control of recombination is implemented progressively in mouse meiosis. *Nature Cell Biol.* **14**, 424–430 (2012).
- de Boer, E., Stam, P., Dietrich, A. J., Pastink, A. & Heyting, C. Two levels of interference in mouse meiotic recombination. *Proc. Natl Acad. Sci. USA* **103**, 9607–9612 (2006).
- Reynolds, A. *et al.* RNF212 is a dosage-sensitive regulator of crossing-over during mammalian meiosis. *Nature Genet.* **45**, 269–278 (2013).
- Chen, S. Y. *et al.* Global analysis of the meiotic crossover landscape. *Dev. Cell* **15**, 401–415 (2008).
- Rosu, S., Libuda, D. E. & Villeneuve, A. M. Robust crossover assurance and regulated interhomolog access maintain meiotic crossover number. *Science* **334**, 1286–1289 (2011).
- Mets, D. G. & Meyer, B. J. Condensins regulate meiotic DNA break distribution, thus crossover frequency, by controlling chromosome structure. *Cell* **139**, 73–86 (2009).

Supplementary Information is available in the online version of the paper.

Acknowledgements We thank A. Dernburg and M. Zetka for antibodies and the CGC (funded by National Institutes of Health (NIH) P40 OD010440) for strains. We thank K. Hillers and K. Zawadzki for comments on the manuscript. This work was supported by a Helen Hay Whitney Foundation Postdoctoral Fellowship, a Katharine McCormick Advanced Postdoctoral Fellowship, and NIH K99 HD076165 to D.E.L. and by NIH R01 GM067268 to A.M.V. B.J.M. is an investigator of the Howard Hughes Medical Institute.

Author Contributions D.E.L. and A.M.V. conceived and designed the experiments, analysed the data and wrote the paper. D.E.L. performed the experiments. S.U. deconvolved confocal images. S.U. and B.J.M. provided scientific discussions and technical expertise for computational straightening of chromosomes.

Author Information Reprints and permissions information is available at www.nature.com/reprints. The authors declare no competing financial interests. Readers are welcome to comment on the online version of the paper. Correspondence and requests for materials should be addressed to A.M.V. (annev@stanford.edu).

METHODS

C. elegans strains, genetics and culture conditions. All strains are from the Bristol N2 background and were maintained and crossed at 20 °C under standard conditions. Temperatures used for specific experiments are indicated in Figures and below.

The following strains were used in this study: (1) AV307: *syp-1(me17) V/nT1 [unc-?(n754) let-? qIs50] (IV;V)*. (2) AV630: *meIs8[unc-119(+)] Ppie-1::gfp::cosa-1] II*. (3) AV647: *meIs8[unc-119(+)] Ppie-1::gfp::cosa-1] II; spo-11(me44) IV/nT1 [unc-?(n754) let-? qIs50] (IV;V)*. (4) AV695: *meIs8[unc-119(+)] Ppie-1::gfp::cosa-1] II; mnT12 (IV;X)*. (5) AV760: *meIs8[unc-119(+)] Ppie-1::gfp::cosa-1] II; unc-24(e138) dpy-4(e1166) mnT12 (IV;X)*. (6) AV761: *meIs8[unc-119(+)] Ppie-1::gfp::cosa-1] II; spo-11(me44) IV/nT1[qIs51] (IV;V)*. Additional information on strains: *qIs50* contains [*Pmyo-2::gfp; Ppes-10::gfp; PF22B7.9::gfp*] and *qIs51* contains [*Pmyo-2::gfp; Ppes-10::gfp; PF22B7.9::gfp*].

For Fig. 4b, c and Extended Data Fig. 6, *meIs8; spo-11 mnT12* worms (and control *meIs8; spo-11/+ mnT12* worms) were obtained by the following scheme: (1) AV761 males × AV760 hermaphrodites; (2) *meIs8; + spo-11 + IV / unc-24(e138) + dpy-4(e1166) mnT12 (IV;X)* males (from cross 1) × AV760 hermaphrodites; (3) progeny from cross 2 were singly plated. *meIs8; + spo-11 + mnT12 / unc-24(e138) + dpy-4(e1166) mnT12 (IV;X)* hermaphrodites were identified on the basis of failure to produce male self progeny, indicating homozygosity for *mnT12*; (4) from step 3 plates that did not produce male progeny, 20–24 h post-L4 non-Unc non-Dpy hermaphrodite progeny were used for immunofluorescence. These included both *spo-11* homozygotes and *spo-11/+* worms, which were used as controls. *spo-11* mutant and control gonads were dissected onto the same slides and were differentiated during imaging based on DAPI-stained bodies in diakinesis-stage oocytes (10 univalents in *spo-11* oocytes and 5 bivalents in controls).

Experimental conditions for partial depletion of SYP-1 by RNAi. For *syp-1* partial RNAi, synchronized L1 larvae (grown at 20 °C from eggs hatched on unseeded plates for 24 h) were placed on fresh NGM + Amp + isopropyl β-D-1-thiogalactopyranoside (IPTG) plates recently seeded with *Escherichia coli* HT115 cells containing either a fragment of the *syp-1/F26D2.2* gene in the L4440 vector, or the empty vector (referred to as control) from the Ahringer laboratory RNAi library²⁸. For analyses of GFP::COSA-1 foci in late pachytene nuclei, hermaphrodite worms were grown at 25 °C starting at the L1 stage and dissected for immunofluorescence at 16–22 h post-L4 stage to obtain optimal SYP-1 depletion for observing an increase in GFP::COSA-1 foci; for quantification of chiasmata, worms were dissected at 24–30 h post-L4 to permit nuclei with optimal SYP-1 depletion in late pachytene at 16–22 h post-L4 to progress to diakinesis. Differences in experimental culture conditions (that is, growth at 25 °C on *E. coli* HT115 on NGM + Amp + IPTG versus growth at 20 °C on *E. coli* OP50 on NGM) likely account for the higher baseline frequency of *mnT12* chromosome pairs with two GFP::COSA-1 foci in the present study (49%) compared to a previous study (30%)⁵.

Evaluation of SYP-1 partial depletion. RNAi partial depletion conditions used for our experiments were consistently and deliberately much less severe than the level of partial SYP-1 depletion used in ref. 9. Under the conditions used for the current work, the vast majority of pachytene nuclei had assembled SCs on all six chromosome pairs and most diakinesis oocytes had chiasmata connecting all six chromosome pairs (see main text). (By contrast, the vast majority of pachytene nuclei analysed in ref. 9 had assembled SCs on only 1, 2 or 3 chromosome pairs, and in the worms used for their crossover analysis, most diakinesis oocytes had multiple achiasmata chromosome pairs⁹.) To assess the extent of partial depletion used in the current study, two different approaches were used, immunoblotting and fluorescence quantification:

Immunoblotting: the extent of SYP-1 depletion achieved by our RNAi conditions was estimated using western blot analysis (Extended Data Fig. 1a). Protein lysates were generated from control, *syp-1* RNAi and *syp-1(me17)* mutant worms (100 worms each; see below). For each experiment, protein blots containing identical amounts of each lysate, plus a dilution series of the control lysate, were probed with α-SYP-1 antibody, and the extent of depletion was estimated by comparing the residual SYP-1 band in the *syp-1* RNAi lysate to the SYP-1 bands in the dilution series from a control lysate processed in parallel.

Protocol details: 100 worms (treated and staged as for the reported immunofluorescence analyses) were picked to unseeded plates, washed off plates with 1.5 ml of cold M9, and spun down at 2,000 r.p.m. for 1 min. After placing on ice for 1 min, supernatant was removed, and worm pellets were washed three times with cold M9 before the addition of 2 × Laemmli buffer with β-mercaptoethanol (Bio-Rad) and boiling for 10 min to create worm protein lysates. Samples of each lysate were run on a 4–15% Bio-Rad TGX acrylamide gel and then transferred to nitrocellulose membrane using a wet Western blot transfer system (Bio-Rad). Membrane was blocked in 5% milk in 1 × Tris Buffered Saline with Tween 20 (TBST) for 1 h at room temperature (approx. 22–23 °C) and then incubated with 1:500 dilution of

rabbit anti-SYP-1 antibody¹² (pre-absorbed with *syp-1(me17)* dissected worms) in 5% milk in 1 × TBST overnight at 4 °C. Membrane was washed 5 × 10 min in 1 × TBST before addition of 1:4,000 dilution of goat anti-rabbit HRP-conjugated antibody in 5% milk in TBST for 2 h at room temperature. Following 5 × 10-min washes in 1 × TBST, membrane was incubated with Clarity Western ECL substrate (Bio-Rad) for 5 min at room temperature and then exposed to film. To assess loading, antibodies were removed from the membrane with mild stripping buffer (Abcam), and the membrane was then blocked, incubated and washed as described above except for the following modification for the primary antibody: 1:10,000 mouse anti-α-tubulin antibody (Sigma no. T6199) in 5% milk in TBST, incubated for 1 h at 4 °C.

Fluorescence quantification: for Extended Data Fig. 1b, c, normalized fluorescence levels were assessed from immunofluorescence slides of control and *syp-1* partial RNAi gonads imaged on the DeltaVision microscope using the imaging conditions described below. During image acquisition, exposure times for channels assessing SYP-1 and HTP-3 fluorescence signals were kept the same for both control and *syp-1* RNAi slides. Deconvolved images were projected using a sum projection algorithm with softWoRx (Applied Precision) software. Using the Edit Polygon tool in softWoRx, individual nuclei from a specific region of the gonad (from two rows before COSA-1 foci formation, to three rows following COSA-1 foci formation) were traced and assessed for SYP-1 and HTP-3 fluorescence intensity. Nuclei were assessed only if they were completely contained within the image stack and did not overlap with any other nuclei in the projected image. (Nuclei with compact DAPI signals indicative of arrest and/or apoptosis were excluded.) Further, a subset of *syp-1* RNAi gonads (40%) that exhibited severe SYP-1 depletion (that is, SYP-1 was not detected on all chromosomes) was excluded from this analysis, as gonads in this category would have been excluded from our experiments evaluating numbers and distribution COSA-1 foci on the basis of presence of asynapsed chromosomes and/or inability to trace continuous chromosome axes (as a result of asynapsis).

For each gonad, background fluorescence in the SYP-1 and HTP-3 channels was assessed by measuring fluorescence intensities for three separate areas between nuclei in the scored region and using these to calculate the average background fluorescence per pixel. For each individual nucleus, SYP-1 and HTP-3 fluorescence measurements were calculated by dividing the total intensity by the total area of the projected nucleus, and then subtracting the average background fluorescence for the gonad. To obtain an average SYP-1:HTP-3 ratio for each gonad, the SYP-1:HTP-3 ratios calculated for each nucleus within a given gonad were averaged. Once average SYP-1:HTP-3 ratios were measured for all gonads, two different approaches were used to compare SYP-1:HTP-3 ratios for *syp-1* RNAi gonads and control gonads: (1) ‘mean of experiments’: for each experiment, the average SYP-1:HTP-3 ratios for control gonads and for *syp-1* RNAi gonads were calculated; the control value was set to 1, and the normalized SYP-1:HTP-3 ratio for *syp-1* RNAi for that particular experiment was expressed as a fraction of the control value. The corresponding graph plots the average normalized SYP-1:HTP-3 ratio for *syp-1* RNAi ± s.d. for three independent experiments; (2) ‘mean of all gonads’: for each individual experiment, the SYP-1:HTP-3 ratio for each individual gonad (both *syp-1* RNAi and control) was normalized to the average control SYP-1:HTP-3 ratio obtained from the same experiment. These values were then used to calculate average (± s.d.) normalized SYP-1:HTP-3 ratios for all control gonads and for all *syp-1* RNAi gonads across all experiments. Note that this latter approach makes it possible to convey the variability in the control measurements in the corresponding graph.

Numbers of gonads assessed: experiment no. 1: control = 7 gonads, *syp-1* RNAi = 7 gonads; experiment no. 2: control = 15 gonads, *syp-1* RNAi = 6 gonads; experiment no. 3: control = 10 gonads, *syp-1* RNAi = 8 gonads.

Of the two approaches, the western blot analysis provides a somewhat lower estimate of residual SYP-1 levels, in part because the subset of worms with more severe SYP-1 depletion (which would have been excluded from our experiments) are included in the protein lysates. Thus, the immunofluorescence approach probably provides a better estimate of the residual SYP-1 levels present in the nuclei analysed in our experiments.

Because our data indicate that a 60–70% reduction in SYP-1 levels can lead to increased COSA-1-marked crossover sites and impaired interference, we also tested whether the *syp-1* locus might be haploinsufficient. As we observed 6.02 ± 0.31 (mean ± s.d., $n = 53$) and 6.00 ± 0.13 (± s.d., $n = 114$) GFP::COSA-1 foci per late pachytene nucleus of *syp-1(me17)/+* and *syp-3(ok758)/+* worms, respectively, we conclude that reducing *syp-1* gene dose by half is not sufficient to impair the robust crossover control system.

Immunofluorescence. Immunofluorescence experiments were performed as described previously²⁹, with modifications. Gonads from adult worms at 18–24 h post-L4 stage were dissected. Slides were mounted with Vectashield (except for confocal images, which were mounted with Invitrogen ProLong Gold) and a

coverslip with a 170 ± 5 - μm thickness. Slides were sealed with nail polish immediately following mounting and stored at 4°C before imaging (except for confocal slides which were cured for 24 h at room temperature before sealing and storing at 4°C). All slides were imaged (as described below) within 2 weeks of preparation. The following primary antibody dilutions were used: rabbit anti-GFP (1:1,000)²; chicken anti-GFP (1:1,000) (Abcam 13970); guinea pig anti-SYP-1 (1:200)¹²; chicken anti-HTP-3 (1:500)³⁰; rabbit anti-HIM-3 (1:200)³¹; guinea pig anti-HIM-8 (1:500)¹⁷.

Imaging. For Fig. 1, immunofluorescence slides were imaged at 512×512 pixel dimensions on an Applied Precision DeltaVision microscope using a $60\times$ objective with $1.5\times$ optivar. Images were acquired as Z-stacks at 0.2 - μm intervals and deconvolved with Applied Precision softWoRx deconvolution software. For Figs 2–4, immunofluorescence slides were imaged at $1,024 \times 1,024$ pixel dimensions on a Leica SP2 AOBs Confocal microscope using a $63\times$ objective with $4.7\times$ zoom in 12-bit format. Images were acquired as Z-stacks at 81 -nm intervals and deconvolved with Huygens Professional deconvolution software (Scientific Volume Imaging). For quantification of GFP::COSA-1 foci, nuclei that were in the last 4–5 rows of late pachytene and were completely contained within the image stack were analysed. Foci were quantified manually from deconvolved three-dimensional stacks. For visualization and quantification of chiasmata (Fig. 1c and Extended Data Fig. 3a), individual *mnT12* bivalents from diakinesis nuclei in -2 , -3 or -4 oocytes were identified on the basis of size, cropped, and rotated in three dimensions using Velocity (PerkinElmer) three-dimensional rendering software. Scoring of chiasmata was primarily on the basis of HTP-3 (chromosome axis) and DAPI staining, as GFP::COSA-1 dissociates from chromosomes during progression through the diakinesis stage. For Fig. 1a, images shown are projections through three-dimensional data stacks encompassing whole nuclei, generated with a maximum-intensity algorithm with the softWoRx (Applied Precision) software. For Fig. 1c, the images shown are snapshots of a Velocity three-dimensional rendering of individual diakinesis bivalents with maximum intensity rendering for HTP-3. Images shown in Figs 2a and 4c are projections through three-dimensional data stacks encompassing whole nuclei, or straightened chromosomes, generated with a maximum-intensity algorithm using Priism/IVE software³².

γ -irradiation experiments. L1 progeny from AV647 worms (heterozygous for *spo-11(me44)* and the *nT1* balancer chromosome) were subjected to RNAi conditions described earlier. *spo-11(me44)* homozygotes were picked at the L4 stage from the RNAi plates on the basis of a lack of dominant markers associated with the balancer and placed on freshly seeded RNAi plates at 25°C . At 12 h post-L4, 25°C *syp-1* and control RNAi-treated worms were γ -irradiated with a Cs-137 source at either 250 rad, 1,000 rad, 2,000 rad, 4,000 rad, 6,000 rad or 10,000 rad. Following γ -irradiation, worms were placed back at 25°C for 8 h until dissection for immunofluorescence. Unirradiated controls were kept at 25°C and dissected at the same time as γ -irradiated worms.

Before quantification of COSA-1 foci, we used SYP-1 immunofluorescence to evaluate the efficacy of SYP-1 partial depletion. In the majority of *syp-1* RNAi gonads (57%), pachytene nuclei had detectable SYP-1 along all six chromosome pairs, but immunofluorescence signals were reduced in intensity relative to controls and there were some small chromosomal regions that lacked SYP-1; gonads in this category ($n = 84$) were used for quantification of COSA-1 foci. Gonads with SYP-1 staining comparable to wild type (18%) and gonads with more severe SYP-1 depletion (that is, SYP-1 was not detected on all chromosomes, 25%) were excluded from this analysis.

For the quantification of COSA-1, the numbers of nuclei counted for each γ -irradiation dose are as follows: control: 0 rad ($n = 189$), 250 rad ($n = 310$), 1,000 rad ($n = 243$), 2,000 rad ($n = 201$), 4,000 rad ($n = 119$), 6,000 rad ($n = 212$), 10,000 rad ($n = 52$); *syp-1* partial RNAi: 0 rad ($n = 138$), 250 rad ($n = 170$), 1,000 rad ($n = 278$), 2,000 rad ($n = 278$), 4,000 rad ($n = 195$), 6,000 rad ($n = 280$), 10,000 rad ($n = 345$).

Measurements along straightened chromosomes and interference analyses.

For quantitative analyses of axis lengths and positions and distributions of COSA-1 foci, *mnT12* chromosomes (identified by HIM-8 binding) and unfused autosomes (from the same nuclei) with continuous and unambiguous chromosome axis staining by either HTP-3 or HIM-3 immunofluorescence were traced in three-dimensions through the centre of the chromosome axis (indicated by strongest staining) and computationally straightened as described before²⁷. Using these straightened chromosomes, the lengths of the chromosome axes and the positions of the HIM-8 focus and COSA-1 foci along *mnT12* were measured using Priism/IVE. The left end of the *mnT12* fusion chromosome (identified based on proximity to the HIM-8 focus) was assigned the zero coordinate, and position coordinates (in μm) were determined and recorded for the centre of the HIM-8 focus, the centres of each COSA-1 focus, and the opposite end of the chromosome axis.

For these analyses, only nuclei in the last four rows of late pachytene that were completely contained within the image stacks were analysed. For the *syp-1* RNAi

gonads analysed, *mnT12* was examined in all nuclei meeting these criteria (115 total *mnT12* chromosomes from 16 gonads, 4 experiments, except for Figs 2d, e and 3, where six *mnT12* chromosomes were omitted from the analyses owing to lack of positional information for proper interval binning). For control analyses where the relative frequencies of *mnT12* chromosomes with 1 versus 2 COSA-1 foci were a relevant factor (Figs 2b, 3a, 4a and Extended Data Fig. 4), we similarly used data from gonads where all nuclei meeting the above-specified criteria were included (69 *mnT12* chromosomes from 6 gonads, 3 experiments, except for Fig. 3a, where one *mnT12* chromosome was omitted from the analyses owing to lack of positional information for proper interval binning). For Figs 2c–e, 3b and 4d, 16 additional control *mnT12* chromosomes with 2 COSA-1 foci from 2 additional gonads were also included in the analyses. Numbers for Fig. 4b: *spo-11/+* control (93 *mnT12* chromosomes from 13 gonads, 5 experiments); *spo-11* (75 *mnT12* chromosomes from 7 gonads, 3 experiments). For Extended Data Fig. 6, data from the same nuclei, plus 20 additional *mnT12* control chromosomes with HIM-8 positional data (from 5 gonads), were included in the analysis. The best-fit linear regression lines in Fig. 4a, b (and corresponding R^2 values) were generated by the Prism graphing program (GraphPad Software). For Fig. 2d, e and Extended Data Fig. 4, positions of foci were normalized by dividing each chromosome into eight intervals of equal size and binning the foci into these eight intervals.

For the interference strength analysis in Fig. 3a, positions of foci were normalized by dividing each chromosome into four intervals of equal size and binning the foci into these four intervals. For each specified pair of intervals tested, this coefficient of coincidence analysis compared the observed frequency of COSA-1 foci occurring in both intervals with the frequency expected if foci occurred independently in the two intervals (that is, absence of interference), with interference strength (I) calculated as $(1 - \text{observed/expected})$. The 'expected' number of chromosomes with COSA-1 foci occurring in both of a given pair of intervals (X and Y) was calculated as: (measured frequency of COSA-1 foci in interval X) \times (measured frequency of COSA-1 foci in interval Y) \times (number of *mnT12* chromosomes examined).

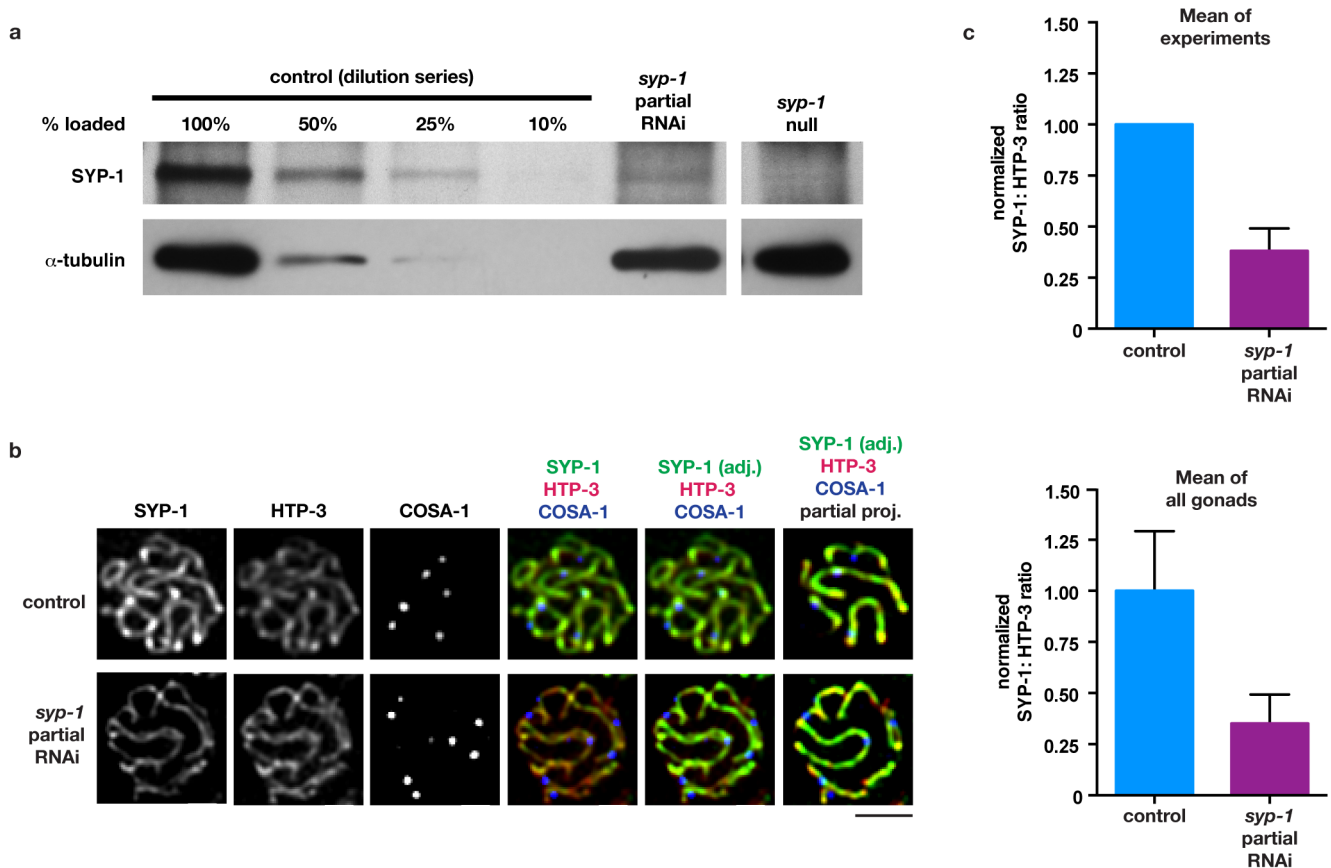
For determining interference strength using the best-fit gamma distribution analyses in Fig. 3b and Extended Data Fig. 5, distances between COSA-1 foci along straightened *mnT12* chromosomes were normalized by calculating the percent axis length separating neighbouring COSA-1 foci. Distances between adjacent foci expressed as per cent axis length were entered into the EasyFit Distribution Fitting Software (Mathwave) to generate histograms of the data sets and best-fit probability distribution curves. Numbers of inter-focus distances used are: control, $n = 47$; *syp-1* RNAi, $n = 183$.

In addition to measuring *mnT12* axis lengths, we also measured axis lengths of unfused autosomes with continuous and unambiguous HTP-3 or HIM-3 staining from the same nuclei used to measure *mnT12*. Numbers of chromosomes analysed were: controls at 25°C (208 autosomes from 62 nuclei, 6 gonads, 3 experiments); *syp-1* RNAi at 25°C (155 autosomes from 58 nuclei, 16 gonads, 4 experiments); *spo-11/+* controls at 20°C (233 autosomes from 77 nuclei, 13 gonads, 5 experiments); and *spo-11* at 20°C (203 autosomes from 62 nuclei, 7 gonads, 3 experiments). As mean axis lengths of unfused autosomes in RNAi controls at 25°C and *spo-11/+* controls at 20°C were nearly identical ($6.42 \pm 0.06 \mu\text{m}$ versus $6.46 \pm 0.04 \mu\text{m}$; \pm s.e.m.), these two data sets were combined to give a single control value for the graph in Fig. 4c.

Statistics. All P values reported in the main text and Extended Data Figs 2 and 6 are two-tailed and calculated from Mann–Whitney tests, which are robust non-parametric statistical tests appropriate for the relevant data sets. For the four-interval data set analysis in Fig. 3a, we used Fisher's exact test (an appropriate test for 2×2 contingency tables) to evaluate (for each pair of intervals) whether COSA-1 foci occurred independently in the two intervals under consideration (Extended Data Table 1). For the two-tailed P value reported in Extended Data Fig. 3b comparing the observed versus expected outcome for GFP::COSA-1 foci within an asynapsed region of the *mnT12* chromosome for *syp-1* RNAi, the χ^2 test was used as it is an appropriate test to compare observed versus expected outcomes for categorical data. For Fig. 4a–c, the goodness-of-fit for the linear regression lines were reported as coefficient of determination (R^2 ; an appropriate goodness-of-fit statistic for fitted linear regression lines), using the Prism graphing program (GraphPad Software). For all tests described above, the assumptions of each test were met.

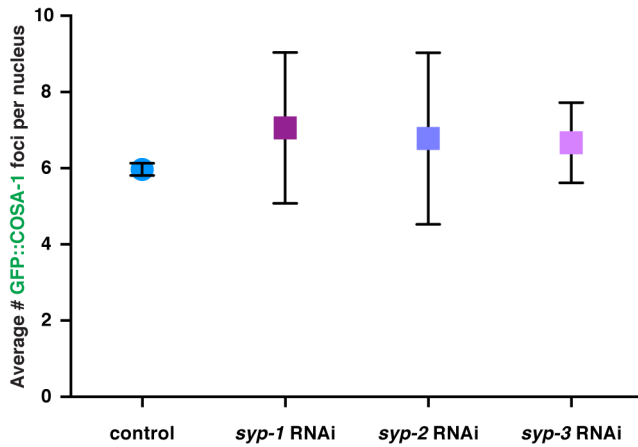
- Kamath, R. S. *et al.* Systematic functional analysis of the *Caenorhabditis elegans* genome using RNAi. *Nature* **421**, 231–237 (2003).
- Martinez-Perez, E. & Villeneuve, A. M. HTP-1-dependent constraints coordinate homolog pairing and synapsis and promote chiasma formation during *C. elegans* meiosis. *Genes Dev.* **19**, 2727–2743 (2005).
- MacQueen, A. J. *et al.* Chromosome sites play dual roles to establish homologous synapsis during meiosis in *C. elegans*. *Cell* **123**, 1037–1050 (2005).

31. Zetka, M. C., Kawasaki, I., Strome, S. & Muller, F. Synapsis and chiasma formation in *Caenorhabditis elegans* require HIM-3, a meiotic chromosome core component that functions in chromosome segregation. *Genes Dev.* **13**, 2258–2270 (1999).
32. Chen, H., Hughes, D. D., Chan, T. A., Sedat, J. W. & Agard, D. A. IVE (Image Visualization Environment): a software platform for all three-dimensional microscopy applications. *J. Struct. Biol.* **116**, 56–60 (1996).

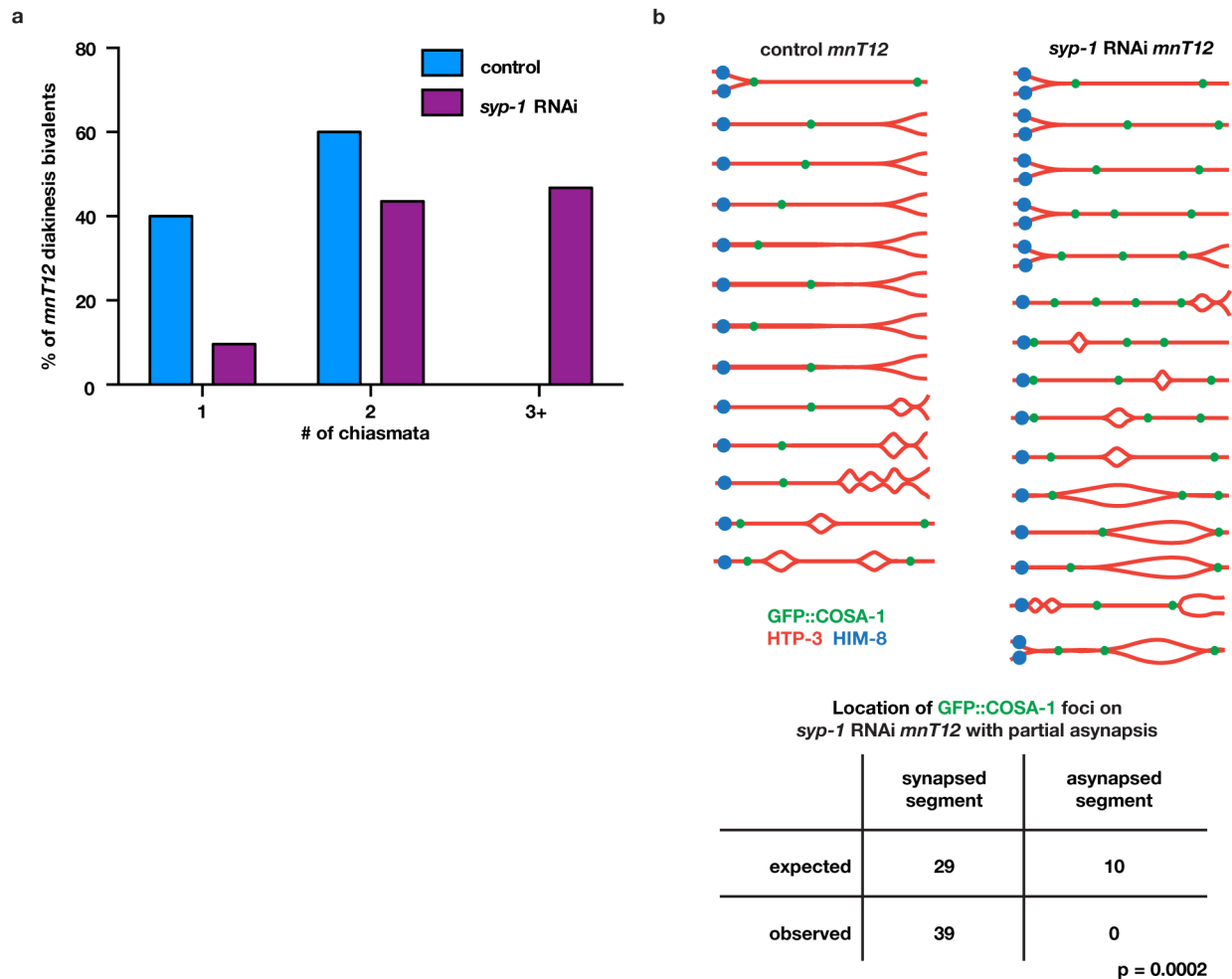


Extended Data Figure 1 | Quantification of SYP-1 partial depletion by attenuated RNAi. **a**, Representative western blot analysis of protein lysates from control, *syp-1* partial RNAi and *syp-1* null worms. A dilution series of control samples was used to estimate that the level of SYP-1 protein was reduced to approximately 25–30% of the control SYP-1 level following *syp-1* partial RNAi under our experimental conditions. All panels shown are from the same membrane probed with indicated antibodies. Similar results were obtained for three independent experiments. **b**, Representative immunofluorescence images of late pachytene nuclei co-stained for SYP-1 (green), chromosome axis marker HTP-3 (red) and GFP::COSA-1 (blue), showing reduction of SYP-1 fluorescence relative to HTP-3 fluorescence and increase in GFP::COSA-1 foci in *syp-1* partial RNAi nucleus compared to control nucleus. Except for right-most panels, images shown are sum projections through three-dimensional data stacks encompassing whole nuclei. For the first four pairs of control and *syp-1* partial RNAi panels, identical

exposure times and dynamic range settings for image display were used to highlight the reduction in the SYP-1:HTP-3 ratio. In the last two panels, SYP-1 signal levels were adjusted for *syp-1* partial RNAi images to facilitate visualization of the SYP-1 tracts. Because some SCs from the top and bottom halves of the nuclei are superimposed in the full projections encompassing whole nuclei, partial projections showing half nuclei are also provided (right-most images). Scale bar, 2 μ m. **c**, Graphs showing quantification of the reduction in SYP-1 fluorescence relative to HTP-3 fluorescence following *syp-1* partial RNAi. Two different methods for analysing the data (see Methods) yield similar results, indicating that under the *syp-1* partial RNAi conditions used for our experimental analysis, SYP-1 levels are reduced to approximately 30–40% of control levels. Error bars indicate s.d. Numbers of gonads assessed: experiment no. 1: control = 7 gonads, *syp-1* RNAi = 7 gonads; experiment no. 2: control = 15 gonads, *syp-1* RNAi = 6 gonads; experiment no. 3: control = 10 gonads, *syp-1* RNAi = 8 gonads.

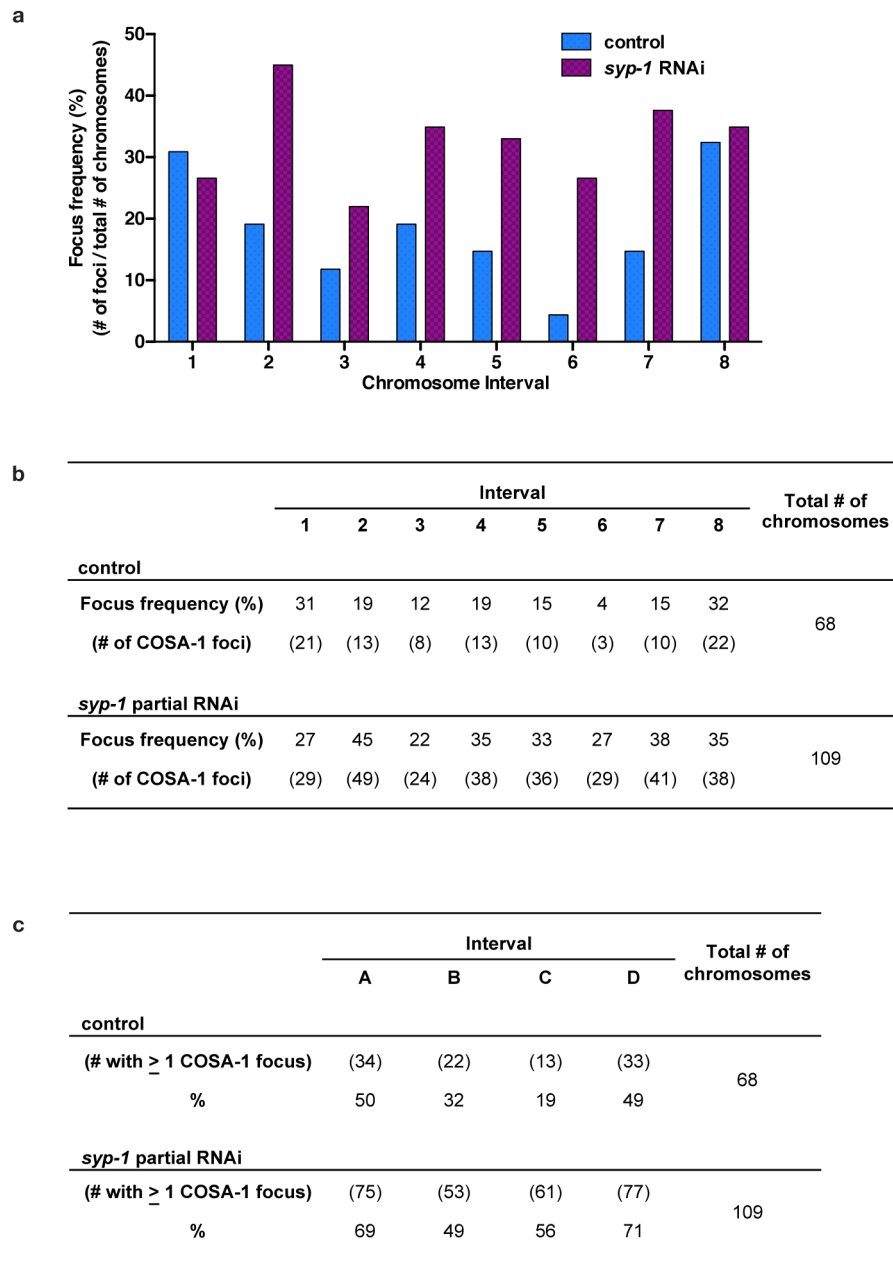


Extended Data Figure 2 | Partial depletion of SYPs increases numbers of COSA-1 foci. Graph depicting the mean numbers of GFP::COSA-1 foci per late pachytene nucleus detected following exposure to *syp-1/F26D2.2*, *syp-2/C24G6.1* or *syp-3/F39H2.4* RNAi or empty vector control²⁸. RNAi and control conditions were identical to those described in Methods, except that worms were dissected for immunofluorescence at 24 h post-L4 stage on RNAi or control plates at 25 °C. Error bars indicate s.d. Control nuclei had an average of six COSA-1 foci per nucleus and a very low standard deviation, indicating operation of the highly robust crossover control system. Partial RNAi treatment for any of the *syp* genes resulted both in a significant increase in the average number of GFP::COSA-1 foci >6 per nucleus (Mann-Whitney, two-tailed $P > 0.0001$ for *syp-1*, *syp-2* and *syp-3* RNAi) and in a much higher s.d., indicating impairment of crossover control. Numbers of nuclei counted were: control, $n = 78$; *syp-1*, $n = 64$; *syp-2*, $n = 129$; *syp-3*, $n = 87$.



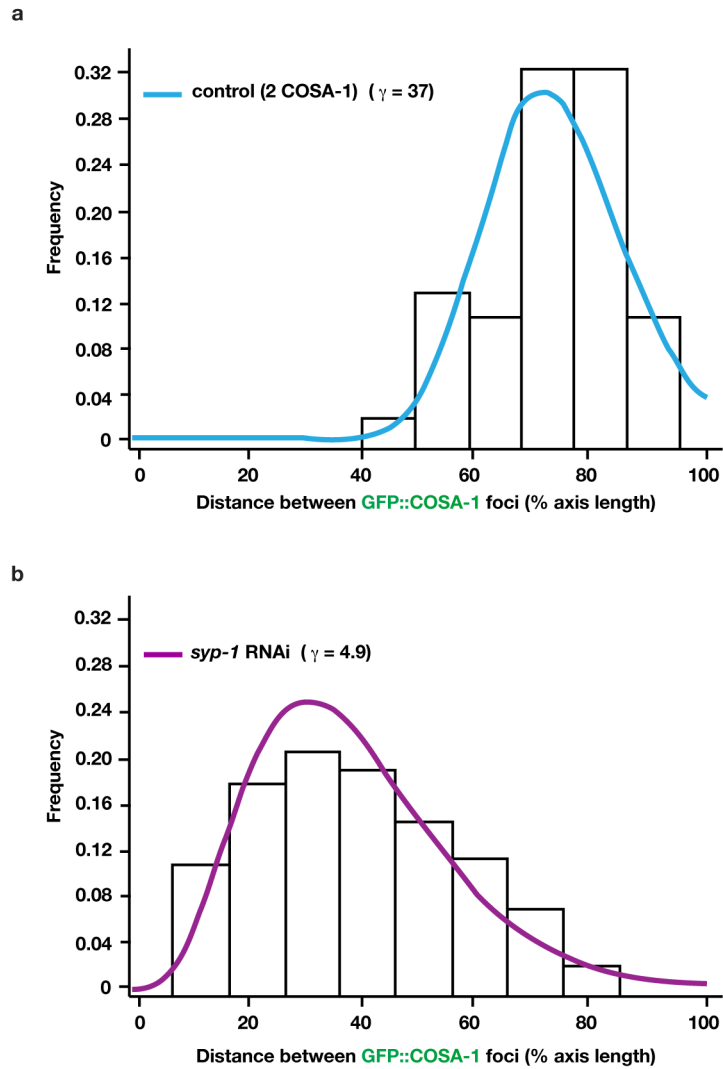
Extended Data Figure 3 | GFP::COSA-1 foci in *syp-1* RNAi nuclei correspond to inter-homologue crossovers. **a**, Quantification of chiasmata on the *mnT12* bivalent in diakinesis-stage oocytes, showing that the incidence of chiasmata corresponds well with the incidence of GFP::COSA-1 foci observed at late pachytene (Fig. 2a). For bivalents with only one or two chiasmata, each individual chiasma was readily scored; bivalents with ≥ 3 chiasmata were pooled into a single category owing to their highly contorted structures, which in some cases made it difficult to discriminate whether 3, 4 or 5 chiasmata were present. In control oocytes, all *mnT12* bivalents had one or two chiasmata. By contrast, 47% of *syp-1* RNAi oocytes had *mnT12* bivalents with ≥ 3 chiasmata, corresponding well with 49% of late pachytene *syp-1* RNAi *mnT12* having ≥ 3 GFP::COSA-1 foci. As formation of each chiasma requires an inter-homologue crossover event, the close correspondence between the numbers of GFP::COSA-1 foci at late pachytene and chiasmata at diakinesis on *syp-1* RNAi *mnT12* bivalents indicates that most, and probably all, GFP::COSA-1 foci in *syp-1* RNAi late pachytene nuclei are marking inter-homologue crossovers. Numbers of diakinesis nuclei scored: control, 86 nuclei from 35 gonads; *syp-1* RNAi, 156 nuclei from 53 gonads. **b**, GFP::COSA-1 foci are not detected on asynapsed chromosome segments. In the regions of the *mnT12* control and *mnT12 syp-1* RNAi germ lines that were imaged for analyses of GFP::COSA-1 foci, we identified a subset of nuclei in which portions of the *mnT12* fusion chromosome pair were asynapsed. These asynapsed segments were found at

comparable frequencies among analysed nuclei from control (8%) and *syp-1* RNAi (12%) germ lines and may represent early stages of desynapsis as cells transition from late pachynema to early diplonema. (Within these nuclei, the asynapsed *mnT12* segments comprised approximately 18% of the total *mnT12* axis length for control and 26% for *syp-1* RNAi.) The *mnT12* bivalents for all control (top left) and *syp-1* RNAi (top right) nuclei in this category are represented in schematic form, with the chromosome axes (HTP-3, red) cartooned to depict both the approximate location and size of the asynapsed segment(s) relative to the total axis length, and the positions of GFP::COSA-1 (green) and HIM-8 (blue) foci. Notably, all GFP::COSA-1 foci on these partially asynapsed chromosome pairs were associated with synapsed segments, located either within a synapsed segment or at the boundary between a synapsed segment and an asynapsed segment; GFP::COSA-1 foci were never found on the asynapsed axis segments. Given the fraction of total axis length that was asynapsed in these *syp-1* RNAi *mnT12* nuclei, the observed restriction of GFP::COSA-1 foci to synapsed segments (where homologues are closely juxtaposed) represents a highly significant (χ^2 test; $P = 0.0002$) departure from the distribution expected if GFP::COSA-1 foci were equally likely to occur on synapsed segments and asynapsed segments (where homologues are separated), consistent with the interpretation that these GFP::COSA-1 foci correspond to inter-homologue recombination events.



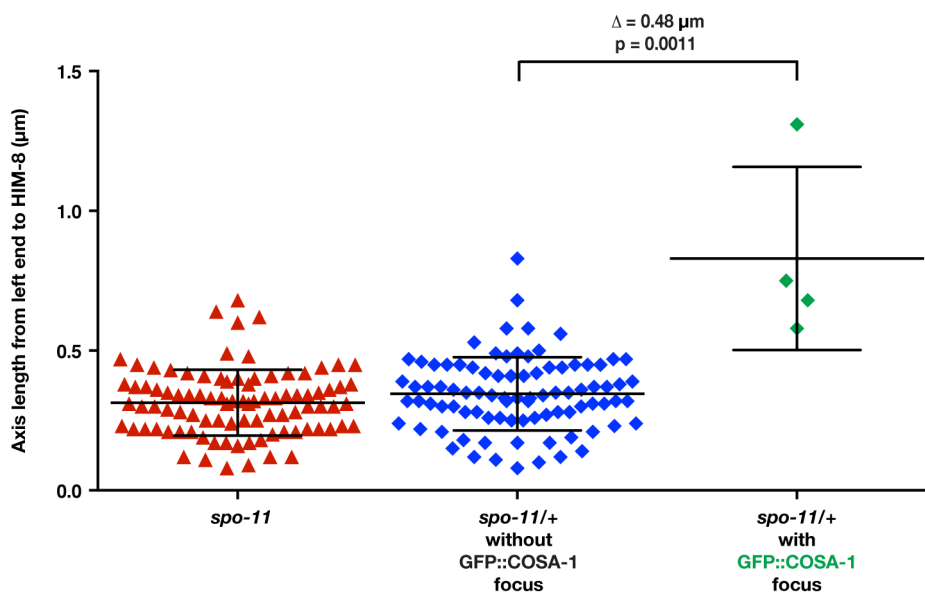
Extended Data Figure 4 | Distribution of GFP::COSA-1 foci among evenly spaced intervals along *mnt12*. **a**, Bar graph for eight-interval analysis of *mnt12* (*X;IV*) fusion chromosomes, indicating the frequencies of GFP::COSA-1 foci in each interval for control (blue) and *syp-1* partial RNAi (purple) worms. **b**, Table for eight-interval analysis indicating both the focus frequencies and the

numbers of GFP::COSA-1 foci in each interval. **c**, Table for four-interval analysis indicating for each interval both the numbers and the percentages of *mnt12* chromosome pairs with ≥ 1 GFP::COSA-1 focus in that interval (used for interference strength calculations in Fig. 3a and Extended Data Table 1).



Extended Data Figure 5 | Gamma probability distribution modelling of inter-COSA-1 focus distances. **a, b,** Histograms of the distribution of inter-focus distances (reported as percentage of total axis length) for binned control

data ($n = 47$) (**a**) and *syp-1* RNAi data ($n = 183$) (**b**). The best-fit gamma probability distribution curves generated from modelling the binned data sets (Fig. 3a) are overlaid on the histograms.



Extended Data Figure 6 | Association between local axis length and GFP::COSA-1 foci at 20 °C. Scatter plot of length measurements (μm) for the segment of *mnT12* chromosome axis from the left end of *mnT12* to the centre of the HIM-8 focus (as seen in Fig. 4d), for *spo-11/+* nuclei without (blue diamonds) or with (green diamonds) a GFP::COSA-1 focus in this chromosome segment and for the *spo-11* mutant (red triangles), which lacks meiotic DSBs and crossovers. Middle lines indicate mean and error bars

indicate s.d. Mean length measurements for *spo-11* nuclei ($0.31 \mu\text{m}$, $n = 92$) and *spo-11/+* nuclei ($0.35 \mu\text{m}$, $n = 88$) lacking a focus in this chromosome segment were not significantly different from each other (Mann–Whitney, two-tailed $P = 0.062$), whereas both were significantly lower (Mann–Whitney, two-tailed $P = 0.0010$; $P = 0.0011$) than for *spo-11/+* nuclei that had a GFP::COSA-1 focus in this segment ($0.83 \mu\text{m}$, $n = 4$).

Extended Data Table 1 | Four-interval analysis of interference.

	Interval Pair					
	AB	BC	CD	AC	BD	AD
control						
Interference Strength (I)	1	1	1	0.68	0.71	-0.81
p-value (Fisher's exact)*	<0.0001	0.0033	<0.0001	0.0115	<0.0001	<0.0001
<i>syp-1</i> partial RNAi						
Interference Strength (I)	0.53	0.6	0.37	-0.1	-0.1	0.09
p-value (Fisher's exact)*	<0.0001	<0.0001	<0.0001	0.067	0.1448	0.2066

* P values from Fisher's exact tests assessing the probability of obtaining the observed data set assuming independent behaviour of the two intervals.